Relativistic tight-binding model: Application to Pt surfaces

A. Tchernatinsky and J. W. Halley

Phys. Rev. B **83**, 205431 — Published 31 May 2011

DOI: 10.1103/PhysRevB.83.205431

Relativistic tight-binding model: Application to Pt surfaces

A. Tchernatinsky and J. W. Halley
University of Minnesota, School of Physics & Astronomy, Minneapolis,MN 55045 USA
(Dated: March 24, 2011)

We report a parametrization of a previous self consistent tight binding model, suitable for metals with high atomic number in which nonscalar relativistic effects are significant in the electron physics of condensed phases. The method is applied to platinum. The model is fitted to DFT band structures and cohesive energies and spectroscopic data on platinum atoms in 5 oxidation states and is then shown without further parametrization to correctly reproduce several low index surface structures. We also predict reconstructions of some vicinal surfaces.

PACS numbers:

I. INTRODUCTION

A great many reactions are catalyzed by platinum but the mechanisms by which the catalysis occurs is not understood in most cases despite enormous theoretical and experimental effort[1] . Technically important chemical reactions on Pt which have been simulated using first principles methods include oxygen reduction[2,3], dehydrogenation of methanol[4,5] and water dissociation[6], for example. However, such first principles calculations cannot simulate the motions of much more than about 100 atoms , although these reactions are very likely to be significantly affected by fluctuating fields arising from water, solvated ions and electronic metallic structure in a larger region of the interface. Furthermore, these first principles calculations have not included all the relevant relativistic effects on the electronic structure in platinum, though near the fermi level these effects are known to be energetically significant for chemical reactions. For example, relativistic effects have been shown to significantly affect the interaction of hydrogen with platinum clusters[7] and determine adsorption properties of carbon monoxide on the Pt $\langle 111 \rangle$ surface[8].

The importance of relativistic effects can also be seen from atomic calculations for Pt using various levels of theory[9]. Upon the inclusion of the spin-orbit interaction approximation to the relativistic Dirac treatment the structure of the valence shell completely changes, as illustrated in Fig. 1. While in non-relativistic simulations the $5d$ state is $\sim 2.8\ eV$ lower than the $6s$ state, when relativity is taken into account the $5d_{5/2}$ becomes the highest occupied state, followed by the $6s_{1/2}$ and $5d_{3/2}$ states.

For these reasons, we have been modeling the surface of Pt and its interactions with H and O using a self consistent semi-empirical electronic structure method called self consistent tight binding (SCTB)[10–20] which permits direct dynamics study of larger systems than can be accessed with full first principles methods. In this paper we describe our method of extending the SCTB method to take account of relativistic effects on the level of the spin-orbit interaction[21] (SO-SCTB). In the next section we describe the general approach. The third section presents results of fitting the SO-SCTB model for platinum to results of first principles calculations on bulk platinum and the fourth section presents results (not fitted) on the relaxed structures of low index faces of platinum as obtained from the relativistic SCTB model. A final section contains discussion, conclusions and an outline of contemplated further work.

II. RELATIVISTIC SCTB

As in the self consistent tight binding (SCTB) method which we developed previously[10–20] the direct dynamics problem is described by the following energy functional (see[10] for the origin of this functional)

$$E_{tot} = \sum_I E_I(\{Q\},\{n\},J_I,\{R\}) \ + \sum_{I\mu,K\nu,\sigma\sigma'} Q_{K\nu\sigma',I\mu\sigma}[\delta_{IK}v_{I\mu,K\nu} + (1-\delta_{IK})t_{I\mu,K\nu}] + \\ + \ \frac{1}{2}\sum_{I\neq K}\frac{e^2(Z_I-Q_I)(Z_K-Q_K)}{R_{IK}}. \tag{1}$$

The only formal difference between this and our previous formulation is in the first, on-site energy functional, term on the right. We are using a tight-binding basis set labeled by capital latin letters $I, K, ..$ representing atomic sites, Greek letters $\mu, \nu, ...$ standing for different atomic orbitals at a given site and σ representing the spin quantum number. The on-site energy function $E_I(\{Q\},\{n\},J_I,\{R\})$ depends self-consistently on local charges $\{Q\}$, on the positions $\{R\}$ of neighbors of the site I and, in the case of the full relativistic model, on configuration occupation

numbers $\{n\}$ and the total ionic angular momentum J_I as described later. In the model including only scalar relativistic effects, $E_I(\{Q\},\{n\},J_I,\{R\})$, does not depend on $\{n\},J_I$ and takes the same form we used in earlier work, namely $E_I = E_{I,\infty}(Q_I) + E_{env}(\{Q\},\{R\})$ where $E_{I,\infty}(Q_I)$ takes account of the electronic structure of the isolated ions at infinite separation. $E_{env}(\{Q\},\{R\})$ is an environmental term which we take, as before, to have the form $E_{env}(\{Q\},\{R\}) = \sum_{n=4}^{11}\sum_{J\neq I} A_n/R_{IJ}^n$ where A_n are fitting parameters which depend on the atomic species present at positions I and J. Formally, the environmental terms could also be included as a part of the matrix $v_{I\mu,K\nu}$ with $K = I$, independent of μ,ν but we do not do that here. The interatomic $v_{I\mu,K\nu}$ terms represent energies arising from electrostatic multipole interactions between the ions of the solid and are treated here exactly as they were in previous work. The kinetic energy matrix elements $t_{I\mu,K\nu}$ are parametrized differently than they were in previous work. Here we use the form[22]

$$t_{I\mu,K\nu} = \frac{(a_{\mu\nu}^{(0)} + a_{\mu\nu}^{(1)}R_{IK} + a_{\mu\nu}^{(2)}R_{IK}^2 + a_{\mu\nu}^{(3)}R_{IK}^3)}{1 + e^{a_{\mu\nu}^{(e)}(R_{IK} - a_{\mu\nu}^{(r)})}} \tag{2}$$

The same form is used for the overlap integrals $s_{I\mu,K\nu}$ which enter the effective one electron equation below. The $Q_{I\mu\sigma,K\nu\sigma'}$ are one body density matrix elements, defined as $Q_{K\nu\sigma',I\mu\sigma} = \sum_\lambda n^\lambda c^*_{I\mu\sigma;\lambda}c_{K\nu'\sigma';\lambda'}$. Here $c_{K\nu'\sigma';\lambda'}$ are the coefficients of a linear combination of the tight binding orbitals labeled by $K\nu'\sigma'$ which give the eigenstate labeled λ' of the effective self consistent one electron Hamiltonian which is obtained by differentiating E_{tot} with respect to the coefficients $c^*_{K\nu'\sigma';\lambda'}$. n^λ is the eigenvalue of the one body density matrix associated with that eigenstate, and is taken in our approximation to be 1 below the fermi level and 0 above it. The parameters in the functions $t_{I\mu,K\nu}$, $v_{I\mu,K\nu}$ and $E_I(\{Q\},\{n\},J_I,\{R\})$ are adjusted so that the band structures and cohesive energies from a series of SCTB calculations on bulk solids with various crystal structures agree with first principles calculations on the same crystals and the energy level structure of the isolated ions matches that known from first principles and/or experiment.

Relativistic effects become important when the speed of the electrons starts to be comparable with that of light. However, valence electrons do not move sufficiently fast for that to happen in any element. Instead, in elements with large atomic number, it is the core electrons that have the most pronounced relativistic effect[23]. As a result of relativistic effects, the effective one electron wavefunction that describes the core state changes, and, because the states of the valence electrons must remain orthogonal to the core states, the wavefunctions of the valence electrons also change. Thus the effects of relativity arise from interactions of the valence electrons with the core and can be represented in the tight binding scheme by modification of the local on-site energy functions $E_{I,\infty}(\{Q\},\{n\},J_I)$. The relativistic information which we use for determining the appropriate onsite functions E_I is embedded in the energies of the low lying many body eigenstates of the platinum atom and of the ions Pt^-, Pt^+. We take these energies from first principles calculations (consistent with experiment) or from atomic spectroscopic experiments as explained in more detail in the next section. We then find that a satisfactory fit to these low lying states of the isolated Pt atom and its ions can be made by causing the function E_I, in the limit in which the ions are very apart so that environmental terms are negligible, to depend on J_I, the total momentum quantum number of the atom or ion, on the occupation numbers of the $5d_{5/2}$ and $5d_{3/2}$ atomic orbitals in the tight binding basis and on the total charge on the ion. Except for this change in the onsite function (described in more detail in the next section) the SCTB model is the same as the one described above for the model including only scalar relativistic effects.

To find the electronic ground state for a given atomic configuration, we minimize the energy functional with respect to the coefficients $c^*_{K\nu'\sigma';\lambda'}$ of the expansion of the one-electron eigenstates in the tight-binding basis. As before, this can be justified by the Hohenberg-Kohn theorem given our energy functional, and gives

$$\frac{\partial E_{tot}}{\partial c^*_{I\mu\sigma;\lambda}} - \varepsilon_\lambda \sum_{K\nu\sigma'} s_{I\mu\sigma,K\nu\sigma'}c_{K\nu\sigma';\lambda} = 0 \tag{3}$$

This gives the effective one electron Schroedinger equations which must be solved self consistently. Here, as before, the second term enforces orthogonality of the one electron eigenfunctions by use of a Lagrange multiplier and $s_{I\mu\sigma,K\nu\sigma'}$ takes account of the possibility that the tight binding basis is non-orthogonal. The effective one-electron Hamiltonian matrix $H_{I\mu\sigma,K\nu\sigma'}$ satisfies

$$\sum_{K\nu\sigma'} H_{I\mu\sigma,K\nu\sigma'}c_{K\nu\sigma';\lambda} = \frac{\partial E_{tot}}{\partial c^*_{I\mu\sigma;\lambda}} \tag{4}$$

$H_{I\mu\sigma,K\nu\sigma'}$ depends on the coefficients $\{c_{J\mu\sigma;\lambda}\}$ and equation 3 is solved self consistently. Relativistic corrections to the effective one electron STCB Hamiltonian appear only from the partial derivatives of the on-site energy function with respect to the new variables J_I, $n_{I,5/2}$ and $n_{I,3/2}$:

$$\sum_{Kj'm'} H^{rel}_{Ijm,Kj'm'}c_{Kj'm';\lambda} = \frac{\partial E_I}{\partial n_{I,5/2}}\frac{\partial n_{I,5/2}}{\partial c^*_{Ijm;\lambda}} + \frac{\partial E_I}{\partial n_{I,3/2}}\frac{\partial n_{I,3/2}}{\partial c^*_{Ijm;\lambda}} + \frac{\partial E_I}{\partial J_I}\frac{1}{2J_I+1}\frac{\partial J_I^2}{\partial c^*_{Ijm;\lambda}}. \tag{5}$$

In this expression we refer to a tight binding basis $|lsjm\rangle$ in which the eigenvalue of the square j^2 of the one electron operator $\vec{j} = \vec{l} + \vec{s}$ is $j(j+1)$, m is the eigenvalue of j_z and the one electron orbital angular momentum quantum number l takes values $l = 0, 1, 2$ in our application. This one electron basis is related to the basis $|lm_l sm_s\rangle$ where m_l and m_s are the eigenvalues of l_z and s_z by the relation $|lsjm\rangle = \sum_{m_l,m_s} C(lsjm; lm_l sm_s)|lm_l sm_s\rangle$ where the $C(lsjm; lm_l sm_s)$ are the appropriate Clebsch-Gordon coefficients, so we can easily pass from one basis to the other. Within this scheme, the quantities $n_{I,5/2}$ and $n_{I,3/2}$ are not uniquely defined because of the well-known ambiguity associated with assigning charge to any particular atom in a condensed system. We have chosen the following, physically plausible definitions, suggested by Mulliken's definition of the charge associated with an atom (as in our other recent SCTB work[16–20]):

$$n_{I,5/2} = \frac{1}{2}\left(\sum_{j=5/2,m,Kj'm'} \left(Q_{Kj'm',Ijm}s_{Ijm,Kj'm'} + Q^*_{Kj'm',Ijm}s^*_{Ijm,Kj'm'}\right)\right) \tag{6}$$

$$n_{I,3/2} = \frac{1}{2}\left(\sum_{j=3/2,m,Kj'm'} \left(Q_{Kj'm',Ijm}s_{Ijm,Kj'm'} + Q^*_{Kj'm',Ijm}s^*_{Ijm,Kj'm'}\right)\right) \tag{7}$$

Here $Q_{Kj'm',Ijm}$ is the one electron density matrix in the $|lsjm\rangle$ basis.

To calculate the square of the total angular momentum J_I^2 of the atom we represent J_I^2 as a sum of the angular momenta $\vec{j}_i$ of the individual electrons labeled by i.

$$\langle J_I^2\rangle = \langle(\sum_i \vec{j}_i)(\sum_i \vec{j}_i)\rangle = \sum_i \langle\vec{j}_i^2\rangle + \sum_{i\neq j}\langle\vec{j}_i\cdot\vec{j}_j\rangle \tag{8}$$

In the language of Hartree Fock theory (e.g.[24]) the first operator on the right is a one-electron operator, while the second operator on the right is a two-electron operator. For the expectation values of these two operators we make the approximation of using the forms which they would take in the Hartree Fock approximation (that is, if the n_λ were the occupancies of orbitals in a Slater determinant):

$$\langle J_I^2\rangle = \sum_\lambda n_\lambda\langle\lambda|\vec{j}^2|\lambda\rangle + \sum_{\lambda\lambda'} n_\lambda n_{\lambda'}(\langle\lambda\lambda'|\vec{j}_1\cdot\vec{j}_2|\lambda\lambda'\rangle - \langle\lambda\lambda'|\vec{j}_1\cdot\vec{j}_2|\lambda'\lambda\rangle) \tag{9}$$

Using the expression $|\lambda\rangle = \sum_{Ijm} c_{Ijm;\lambda}\phi_{Ijm}$, $\langle J^2\rangle$ then takes the form

$$\langle J_I^2\rangle = \sum_{Kjm,K'j'm'} Q_{K'j'm',Kjm,}\langle Kjm|\vec{j}^2|K'j'm'\rangle + \tag{10}$$

$$\sum_{Kjm,K'j'm'K''j''m'',K'''j'''m'''} Q_{K''j'',m'',Kjm}Q_{K'''j'''m''',K'j'm'}\times \tag{11}$$

$$(\langle Kjm,K'j'm'|\vec{j}_1\cdot\vec{j}_2|K''j''m'',K'''j'''m'''\rangle -$$
$$\langle Kjm,K'j'm'|\vec{j}_1\cdot\vec{j}_2|K'''j'''m''',K''j''m''\rangle)$$

In this expression all small j's are associated with the site I , so that the matrix elements will be non-zero only if $K = K' = K'' = K''' = I$. In the following discussion leading to an expression for the last term in Eq. (5), we omit the site index I for simplicity. To compute $\langle J_I^2\rangle$ we need the angular momentum matrix elements

$$\langle jm|\vec{j}^2|j'm'\rangle = j(j+1)\delta_{jj'}\delta_{m,m'}. \tag{12}$$

and in the second term expressing $\vec{j}_1\vec{j}_2$ as

$$\vec{j}_1\cdot\vec{j}_2 = j_1^z j_2^z + \frac{1}{2}(j_1^+ j_2^- + j_1^- j_2^+) \tag{13}$$

the matrix element is given by

$$\langle jm,j'm'|j_1^z j_2^z + \frac{1}{2}(j_1^+ j_2^- + j_1^- j_2^+)|j''m'',j''',m'''\rangle = \tag{14}$$
$$mm'\delta_{jj''}\delta_{m,m''}\delta_{j'j'''}\delta_{m',m'''} +$$
$$\frac{1}{2}\sqrt{j(j+1)-m''(m''+1)}\sqrt{j'(j'+1)-m'''(m'''-1)}\delta_{jj''}\delta_{m,m''+1}\delta_{j'j'''}\delta_{m',m'''-1} +$$
$$\frac{1}{2}\sqrt{j(j+1)-m''(m''-1)}\sqrt{j'(j'+1)-m'''(m'''+1)}\delta_{jj''}\delta_{m,m''-1}\delta_{j'j'''}\delta_{m',m'''+1}$$

A similar expression is found for the exchange term, with the double primed indexes exchanged with triply primed ones. Putting these matrix elements into Eq. (11), we obtain

$$\begin{aligned}\langle J^2\rangle = \sum_{jm} Q_{jm,jm} j(j+1) + \\ \sum_{jm,j'm'} (Q_{jm,jm}Q_{j'm',j',m'} mm' + \\ Q_{jm-1,jm}Q_{j'm'+1,j'm'}\frac{1}{2}\sqrt{j(j+1)-m(m-1)}\sqrt{j'(j'+1)-m'(m'+1)} + \\ Q_{jm+1,jm}Q_{j'm'-1,j'm'}\frac{1}{2}\sqrt{j(j+1)-m(m+1)}\sqrt{j'(j'+1)-m'(m'-1)} - \\ Q_{j'm',jm}Q_{jm,j'm'} mm' - \\ Q_{j'm'+1,jm}Q_{jm-1,j'm'}\frac{1}{2}\sqrt{j(j+1)-m(m-1)}\sqrt{j'(j'+1)-m'(m'+1)} - \\ Q_{j'm'-1,jm}Q_{jm+1,j'm'}\frac{1}{2}\sqrt{j(j+1)-m(m+1)}\sqrt{j'(j'+1)-m'(m'-1)})\end{aligned} \tag{15}$$

Using the Hermitian property of the one electron density matrix:

$$Q_{jm,j'm'} = Q^*_{j'm',jm} \tag{16}$$

we simplify this to

$$\begin{aligned}\langle J^2\rangle = \sum_{jm} Q_{jm,jm} j(j+1) + \left(\sum_{jm} Q_{jm,jm} m\right)^2 + \\ |\sum_{jm} Q_{jm-1,jm_j}\sqrt{j(j+1)-m(m-1)}|^2 - \sum_{jm,j'm'} (Q_{jm,j'm'}Q_{j'm',jm} mm' + \\ Re(Q_{j'm'+1,jm}Q_{jm-1,j'm'})\sqrt{j(j+1)-m(m-1)}\sqrt{j'(j'+1)-m'(m'+1)}\Big)\end{aligned} \tag{17}$$

Now it is fairly straightforward to calculate relativistic correction to the Hamiltonian in Eq.(5)

$$\begin{aligned}H^{rel}_{Ijm,Kj'm'} = \frac{\partial E}{\partial n_{I,5/2}}\frac{1}{2}(S_{Ijm,Kj'm'} + S^*_{Kj'm',Ijm})\delta_{jj'}\delta_{j5/2} + \\ \frac{\partial E}{\partial n_{I,3/2}}\frac{1}{2}(S_{Ijm,Kj'm'} + S^*_{Kj'm',Ijm})\delta_{jj'}\delta_{j3/2} + \\ \frac{\partial E}{\partial J_I}\frac{1}{2J_I+1}\delta_{IK}\left\{ j(j+1)\delta_{jm,j'm'} + 2m\left(\sum_{j''m''} Q_{Ij''m'',Ij''m''}m''\right)\delta_{jm,j'm'} + \right. \\ \left(\sum_{j''m''} Q_{Ij''m''-1,Ij''m''}\sqrt{j''(j''+1)-m''(m''-1)}\right)\sqrt{j(j+1)-m(m+1)}\delta_{jm,j'm'-1} + \\ \left(\sum_{j''m''} Q^*_{Ij''m''-1,Ij''m''}\sqrt{j''(j''+1)-m''(m''-1)}\right)\sqrt{j(j+1)-m(m-1)}\delta_{jm,j'm'+1} - \\ Q_{Ijm,Ij'm'}mm' - \\ Q_{Ij'm'+2,Ijm}\sqrt{j(j+1)-m(m-1)}\sqrt{j'(j'+1)-(m'+1)(m'+2)} - \\ \left. Q_{Ij'm'-2,Ijm}\sqrt{j(j+1)-m(m-1)}\sqrt{j'(j'+1)-(m'-1)(m'-2)}\right\}\end{aligned} \tag{18}$$

One can choose various criteria of self consistency for the solutions of the resulting set of effective one electron equations. One can require that the entire density matrix $Q_{I\mu,K\nu}$ be self consistent. In our non-relativistic SCTB we

only imposed the less stringent requirement that the local charges be self consistent. In the present implementation of the SCTB with relativistic effects we found it sufficient to require self consistency of the local density matrix $Q_{Ijm,Ij'm'}$ at each site, of the occupancies $n_{I,5/2}$ and $n_{I,3/2}$ at each site and of the local charge at each site. Note that the self consistency of $Q_{Ijm,Ij'm'}$ does not imply the self consistency of $n_{I,5/2}$ and $n_{I,3/2}$ because the latter depend on density matrix elements which are not site diagonal, through the Mulliken definition. On the other hand the self consistency of J^2 is guaranteed by the self consistency of $Q_{Ijm,Ij'm'}$.

III. APPLICATION TO PT

To apply the formulation just described to make a model of platinum metal, we first fit a SCTB model without the extra terms in the onsite function described in section II to results of DFT calculations using the Vienna AbInitio Simulation Package (VASP)[25–27] taking account of only scalar relativistic effects (SR-VASP) giving a tight binding model which we call SR-SCTB. We then took account of spin orbit interaction by use of the refined onsite function described in the preceding section to get a fully relativestic model called SO-SCTB. The database for the SR-SCTB model consisted of ionization potentials of the platinum atom and of cohesive energies and band structures obtained from plane wave DFT calculations in LDA approximation (SR-VASP) for a set of atomic configurations. For the SO-SCTB model, energies of a series of excited states of the platinum atom and ions as well as some information from VASP calculations on bulk Pt including spin orbit interaction (SO-VASP) were added to the database.

The first two ionization potentials of Pt are experimentally known to be 9.0 eV and 18.6 eV. We performed calculations of the ionization potentials at various level of theory with the G03 software[28] and found the best agreement with the experimentally known values was given by the quadratic configuration interaction (CI) method (keyword QCISD(T)) with SDD basis set[29] (see Table I). We used that method to calculate the third and fourth ionization potentials. The first electron affinity of a neutral, isolated Pt atom of 2.13 eV has been measured[30] and approximately confirmed by our Gaussian03 calculations (Table I.).

The database of ionization potentials used in the fit for the isolated platinum part of the onsite energy function of the SR-SCTB model are summarized in Table I . In the SR-SCTB model including only scalar relativistic effects, these values were fit to a polynomial of sixth degree in the charge. (The coefficient of the Q^6 term was fixed at +0.01 to assure model stability.)

TABLE I: Ionization potential values as calculated by G03 and experimental data.

Q,e	-1	0	1	2	3	4
I(G03),eV	-1.8	0.0	8.3	17.9	29.7	46.1
I(Exp),eV	-2.13	0.0	9.0	18.6	-	-
I(Model),eV	-2.13	0.0	9.0	18.6	29.7	46.1

Having determined the part $E_\infty(Q)$ of the onsite function for the scalar-relativistic case, we then used the other parameters in the energy functional (2) to fit SR-SCTB calculations to results of first principles calculations of band structures and cohesive energies of a set of atomic distortions of FCC and BCC bulk platinum. The SR-VASP calculations were performed using the local density functional of Ceperley and Adler as parametrized by Perdew and Zunger[32], a k-point grid of 11×11×11 generated with the Monkhorst and Pack algorithm[33], and an energy cutoff of 500 eV. The Projector-Augmented-Wave (PAW) approximation was used to represent core electrons.

By applying a Monte-Carlo fitting procedure, we obtain a set of parameters for Pt metal. Fig. 2 compares the SR-VASP and fitted SR-SCTB results for the dependence of the energy relative to the ground state versus atomic volume for FCC and BCC bulk platinum. Cohesive energies for the ground state are 7.22 eV per atom (SR-VASP) and 7.21 eV (SR-SCTB) and 5.8 eV (experiment). Overestimation of the cohesive energy is a well-documented feature of the LDA approximation. The equilibrium lattice constants are 3.91 Å(SR-VASP), 3.91 Å(SR-SCTB) and 3.90 Å(experiment). The result of the fit for the band structure of the FCC Pt metal at the equilibrium lattice constant is shown in Fig. 3. Results from the fit for cohesive energies of bulk solid containing longitudinal and transverse phonon distortions corresponding to frozen acoustic phonons at the X and L points of the fcc Brillouin zone (zone boundary in the $\langle 001\rangle$ and $\langle 111\rangle$ directions) are shown in Fig. 4. Fitting to such short wave length distortions was found in our earlier SCTB model of titanium metal to be essential if the model is to give reasonable atomic relaxation and dynamic behavior.

To fit the SO-SCTB model, we determined a data base of spectroscopic energies for the three ionization states of Pt as described in detail in the Appendix. Using these, the onsite term in terms $E_\infty(Q, n_{3/2}, n_{5/2}, J)$ in the onsite

SO-SCTB Hamiltonian were parametrized at discrete values $m|e|$ of the charge Q by the form

$$E_\infty(Q = m|e|, n_{3/2}, n_{5/2}, J) = C_m - \sum_{terms\ i} B_i e^{(w_m((n_{3/2}-n_{i,3/2})^2+(n_{5/2}-n_{i,5/2})^2+(J-J_i)^2))} \tag{19}$$

Here, all the parameters except the w_m could be fit using the spectroscopic data alone. However, as explained in more detail in the Appendix, the w_m which describe how the energies vary when the values $n_{3/2}, n_{5/2}, J$ differ from the values they take in the isolated ions and atom, could not be so determined. (The w_m play a role somewhat like a Hubbard U.) To estimate the w_m, we computed bulk Pt cohesive energies and band structures using VASP with the SO tag LSORBIT set to 'ON' (SO-VASP). The method by which the SO interaction is taken into account by this SO-VASP calculation is described in reference[31] . It is not fully consistent with the way we are treating the SO interaction in SO-SCTB (and the SO-SCTB representation of this aspect should actually be more complete) , so this estimate of the w_m is not completely consistent. This may be the reason for the fact that there are some discrepancies between the final SO-SCTB and the SO-VASP cohesive and band energies (Fig. 5), cohesive energies as a function of atomic volume (Fig. 6) and cohesive energies as a function of lattice distortions (Fig. 7) . In spite of the caveats, the SO-VASP database for bulk Pt is represented quite well by the SO-SCTB model . For example, the spin-orbit splitting of about 1 eV in the d-band at the Γ point is well represented. Comparison of Figures 2 and 6 as well as of 4 and 7 shows that, in both the VASP calculations and the fit SCTB calculations, the addition of nonscalar relativistic effects does have a significant effect on the bonding as well as on the band structure.

IV. PT SURFACES

Here we describe application of the SR-SCTB and SO-SCTB models for platinum to the description of low index metal-vacuum surfaces. No further fitting of the SCTB models was done in these surface calculations. We describe results for unreconstructed low-index surfaces, for which a variety of different calculations is available[34], for the reconstructions of low-index surfaces (including the 5×29 reconstruction of the $\langle 001\rangle$ surface for the first time) and for the vicinal $\langle 210\rangle$ and $\langle 310\rangle$ surfaces.

We performed the surface calculation in a slab geometry: The surface was represented by a supercell consisting of a thin film of the material along with vacuum, periodically repeated in all 3 directions. The surface energy E_s was calculated using the relation

$$E_s = \frac{1}{2}(E_{slab} - nE_{bulk}) \tag{20}$$

where E_{slab} is the total energy of the slab, while E_{bulk} is a cohesive energy per atom of FCC Pt. Accurate determination of E_{bulk} is crucial, as was shown in[37]. We verified that the bulk energy obtained by the method proposed in[37] is in agreement with the one calculated by the true bulk simulation.

For the low-index surfaces, a slab with 9 atomic layers was used, with 9 layers of vacuum. We found that this thickness is sufficient to calculate the energy surface to within 0.05 eV/atom. For description of atomic relaxation and dynamics, we used the Γ point approximation, in order to conveniently permit the study of a disordered liquid (such as water) on the surface at a later stage.

Our results indicate that a supercell about 9 times the size of the elementary surface unit cell in both directions along the surface is required. Surface energies at these sizes are convergent to within 0.05 eV. Calculations with the SO-SCTB model were performed by utilizing BZ summation over the 9×9 k-grid. Full structural relaxation is performed as well.

We present results for unreconstructed, relaxed, low index surfaces in Table II, where they are compared with results of first principles[34,36] (FLAPWLDA,PAWGGA) and another tight tight binding[34](NRLTB) calculation reported in the literature. In Table II we report surface energies and changes in the interplanar distances between first and second atomic layers ($\triangle d_{12}$) and second and third atomic layers ($\triangle d_{23}$). The $\langle 111\rangle$ surface is found to have the lowest surface energy, followed by $\langle 001\rangle$ and $\langle 011\rangle$. This order of surface energies is also expected from a simple bond-breaking picture. Relaxation of atomic positions is found to be very small for the $\langle 111\rangle$ and $\langle 001\rangle$ surfaces, while the $\langle 011\rangle$ surface relaxes quite appreciably. Overall there is a very good agreement between surface energies calculated with our SR-SCTB model and the first principles FLAPWLDA and PAWGGA calculations(with no fitting). SR-SCTB surface energies are slightly lower than the first principles ones. Structural parameters are also in the very good agreement with the FLAPWLDA results. The discrepancy between our results and the PAWGGA ones probably arises because PAWGGA used the generalized gradient approximation (GGA) whereas our SR-SCTB was fitted to SR-VASP calculations on bulk Pt which used DFT in the local density approximation (LDA). Surface energies reported[36] using the GGA are lower than those which were reported[34] using LDA, in agreement with a common tendency of the LDA to give larger bonding energies than the GGA.

The quality of the NRLTB surface energy results is similar to ours. Our SR-SCTB derived structural parameters agree with reported DFT results[34,36] somewhat better than do those of the NRLTB model as reported in reference[34]. The NRLTB model uses a simpler representation of the spin orbit interaction effects than our SO-SCTB model. NRLTB represents the spin orbit interaction with an effective one-electron spin-orbit operator.

We also determined the nature of the surface states on the 111 surface within the SO-SCTB model for comparison with experimental data from reference[38]. We found that the energy of the calculated surface states was a sensitive function of slab thickness. The results shown in Figure 8 were obtained with a slab 24 layers thick. The two surface states behave similarly to the experimentally observed ones (see Figure 4 (a) of reference[38]), though the energy of the surface states at the surface $\bar{\Gamma}$ point is almost 0.5eV farther above the fermi energy than the experimentally observed ones. However we found that the energy of the surface states at the $\bar{\Gamma}$ point was smaller when we used the 24 layer slab than when we used a 9 layer slab and we have not done any more calculations at still thicker slabs to check for convergence. Each of the calculated surface states is doubly degenerate and we checked, by looking at the wave functions, that this is because there is one state of each type on each slab surface. The spin nature of the calculated surface states is complicated and different for the two surface states. It can be further analysed from the wave functions but we have not yet done that. The energy splitting of the two calculated surface states is quantitatively quite similar to the experimentally observed splitting. Of course a comparison of the Kohn Sham like states of our self consistent tight binding calculation with experimentally observed spectra of states excited in scanning tunneling microscopy has not been fully justified on theoretical grounds and the comparison is only suggestive.

TABLE II: Surface energies and atomic layers separation changes for low index Pt surfaces. The first set of data is from calculations using our SR-SCTB model, the second set (SO-SCTB) is from our SO-SCTB model, the third set (FLAPWLDA) are first principles results reported in[34], the fourth set(PAWGGA) is first principles results from [36]. The fifth set (NRLTB) is results from the Naval Research Lab Tight-Binding model[34].Finally we include (CALDA) an LDA calculated surface energy for $\langle 111 \rangle$ reported in[35]

Method		$\langle 111 \rangle$	$\langle 001 \rangle$	$\langle 011 \rangle$
SR-SCTB	E_s(eV/atom)	0.96	1.39	1.84
	$\triangle d_{12}$(%)	+1.6	-1.8	-12.0
	$\triangle d_{23}$(%)	0.0	-0.8	+6.5
SO-SCTB	E_s(eV/atom)(with SO)	0.83	1.25	1.57
	$\triangle d_{12}$(%)	+2.0	-1.9	-13.8
	$\triangle d_{23}$(%)	0.0	-0.5	+8.1
FLAPWLDA	E_s(eV/atom)	1.10	1.49	2.16
	$\triangle d_{12}$(%)	+1.3	-1.9	-14.0
	$\triangle d_{23}$(%)	+0.3	+0.2	+8.3
PAWGGA	E_s(eV/atom)	0.55	1.28	-
	$\triangle d_{12}$(%)	+0.99	-2.54	-
	$\triangle d_{23}$(%)	-0.49	-0.47	-
NRLTB	E_s(eV/atom)	0.98	1.45	2.04
	$\triangle d_{12}$(%)	+3.8	-0.5	-16.7
	$\triangle d_{23}$(%)	+0.2	+0.4	+12.4
CALDA	E_s(eV/atom)	0.74		

We also made calculations within the SO and SR-SCTB models to determine the energy and stability of the missing row reconstruction on the $\langle 011 \rangle$ surface and the hexagonal reconstruction on the $\langle 001 \rangle$ surface. A picture of the $\langle 011 \rangle$ reconstructed surface is presented in Fig. 9. Reconstruction energies E_{rec}, defined as the negative of the change in surface energy per surface unit cell due to reconstruction, and structural parameters are presented in Table III. Again, we compare our SR-SCTB results with the FLAPWLDA and NRLTB results reported in[34]. The SR-SCTB produces structural parameters and surface energy in agreement with the FLAPWLDA results for this surface. However when we calculated the reconstruction energy using SO-SCTB we found a much larger value, consistent with the results of[39], which reports that the Pt $\langle 011 \rangle$ surface does not reconstruct if relativistic effects are not taken into account. The origin of the higher surface energy for SO-SCTB is likely to be in the larger bond energies, as compared with SO-VASP which one sees in the fit to the bulk lattice distortions in Figure 7. As we have mentioned above and in the Appendix, these discrepancies arise because the SO-SCTB model uses spectroscopic data, rather than calculated effective one electron spin orbit parameters, to characterise the non scalar relativistic effects. It appears possible that the SO-SCTB therefore gives a more complete description of the nonscalar relativistic effects.

TABLE III: Energetic and structural parameters of the ⟨011⟩ missed row reconstruction. Structural parameters are depicted in Fig. 9

	SR-SCTB	SO-SCTB	FLAPWLDA[34]	NRLTB[34]
E_{rec}(eV/Surface unit cell)	0.18	0.74	0.24	0.47
$\triangle d_{12}$(%)	-15.7	-14.7	-18.8	-26.0
$\triangle d_{23}$(%)	-1.4	-1.9	+0.5	-3.7
$\triangle d_{34}$(%)	+3.3	+3.6	+1.7	-1.5
δ_3(Å)	0.33	0.32	0.28	0.42
P_2(Å)	0.02	0.02	0.04	0.05
P_4(Å)	0.08	0.05	0.07	0.08

Hexagonal reconstruction of the ⟨001⟩ surface has been studied experimentally by LEED[40–43] and more recently by STM[44,45] as well as theoretically[46–49]. Experimental studies suggest the following sequence of the reconstructions: 1×1, followed by metastable 5×1, followed by 5×20 and finally by rotated $5 \times 20R0.7^o$. 5×20 here is merely an established notation, as the actual periodicity along y-direction cannot be precisely determined from the experiment. Theoretical studies using DFT methods[47,49] are limited to the 5×1 reconstruction due to system size constraints. While detailed study of all possible variants of this reconstruction is beyond the scope of this paper, we used the SR-SCTB model to calculate the relaxed surface energies of the 5×1 structure and of the 5×29 reconstruction recently suggested on the basis of experimental STM[45] data for the nominal '5×20' reconstruction. In both cases we used a surface slab of 5 atomic layer instead of the 9 layers used in the low index face relaxation studies, in order to reduce computational cost. The results of our SR-SCTB calculations for the hexagonal reconstructions are presented in Table IV, along with the results of DFT calculations[47,49] by others and an experimental result for the surface energy[41]. One can see that the SR-SCTB results for geometrical properties, like surface corrugation and the interplanar distance change are in very good agreement with the DFT results for the 5×1 reconstruction. The SR-SCTB 5×1 reconstruction energy is almost 0.4 eV/atom higher than the one reported for the DFT calculation. Our SR-SCTB calculation of the 5×29 reconstruction energy is quite close to the value reported experimentally for the hexagonal reconstruction[41]. The structure of the SR-SCTB derived reconstructions is also somewhat different from that obtained from DFT calculations, as shown in Fig. 10. The atom in the center of symmetry of the surface layer, marked by black color, appears in the SR-SCTB result to be the closest to the second layer, unlike the the DFT results[47,49]. We also observed some reconstruction in the second layer, which was not reported by the first principles calculations[47,49]. There is some experimental evidence for reconstruction of the second layer in this surface[45]. Finally, we find in the SR-SCTB calculation that the 5×29 reconstruction, which could not be studied using DFT because of size constraints, has the lowest surface energy , consistent with the experimental result[41]. We find that the SR-SCTB 5×1 surface energy is lower than the 1×1 SR-SCTB surface energy, but higher than 5×29 SR-SCTB surface energy. This supports the suggestion that the 5×1 reconstruction is a metastable state[42].

TABLE IV: Energetic and structural parameters of the ⟨001⟩ hexagonal reconstruction relative to the 5×1 unit cell of the unreconstructed surface. Comparison is with DFT(LDA)[49] and DFT(GGA)[47] simulations and experimental results[41]

	SR-SCTB (5×1)	SR-SCTB (5×29)	DFT(LDA) (5×1)	DFT(GGA) (5×1)	Expt Expt
E_{rec}(eV/atom)	0.74	1.05	0.35	0.25	1.05
$\triangle d_{12}$(%)	+19.2	+19.5	+18.8	+19.0	
Surf. corr. (Å)	0.3	0.6	0.4	0.38	

Finally, we applied our SR-SCTB model to calculate surface energies of the vicinal surfaces ⟨210⟩ and ⟨310⟩. Vicinal surfaces are of interest because they serve as models for the steps on the surfaces of micro and nanoparticulate Pt used as catalysts[50]. The results of our calculations are presented in Table V For comparison, results of density functional calculations within GGA approximation are presented for the ⟨210⟩ surface[51]. One observes that the surface energy of the ⟨210⟩ surface as calculated by SR-SCTB is 3.03 eV per surface atom, in contrast to the result[51] of 2.04 eV/atom. The discrepancy probably arises because reference 47 used the GGA which seems to consistently produce[34,52] surface energies lower than the LDA approximation. In any case our SR-SCTB model was parametrized

by fitting to bulk properties of Pt calculated using LDA so the SR-SCTB model should reproduce LDA, not GGA, results. The interplanar distances for the ⟨210⟩ surface are, on the other hand, quite similar when determined from SR-SCTB and the GGA calculations of reference 47. We found no published DFT results for the ⟨310⟩ surface and may regard our SR-SCTB as predictions to be compared with future experiments.

TABLE V: Properties of ⟨210⟩ and ⟨310⟩ surfaces as calculated with SCTB. ⟨210⟩ surface is compared with DFT(GGA)[51]

	⟨210⟩ SR-SCTB	⟨210⟩ SO-SCTB	⟨210⟩ DFT(GGA)	⟨310⟩ SR-SCTB	⟨310⟩ SO-SCTB
E_s(eV/atom)	3.03	2.74	2.04	4.30	3.74
$\triangle d_{12}$(%)	-21.7	-20.1	-28.9	-7.9	-16.7
$\triangle d_{23}$(%)	-4.2	-6.2	-2.9	-28.7	-27.0
$\triangle d_{34}$(%)	+11.8	+14.8	+15.5	-1.7	-21.0
$\triangle d_{45}$(%)	-6.2	-8.5	-7.7	+19.4	+20.1

To evaluate the computational performance of the SO-SCTB model for platinum we made tests on one surface unit cell of the ⟨111⟩ surface of spin-polarized, relativistic Pt, consisting of 9 atomic layers, with a 9×9 k-point grid. The time required to make one self consistency step with the SCTB model was 42 seconds, while the corresponding DFT VASP calculation was done in 420 sec, so the SCTB was about an order of magnitude faster. Similarly, memory requirements for SO-SCTB differed by an order of magnitude in this test: the SO-SCTB calculation required 0.2 Gb of RAM , while the VASP calculation required 2.1 Gb .

V. CONCLUSIONS

We have developed a SCTB model for Pt metal in two variants: a scalar-relativistic model (SR-SCTB) and a model including spin-orbit approximation (SO-SCTB) which actually goes beyond the usual formulation of the spin orbit interaction by implicitly including all of the relativistic effects manifest in the lowest lying spectroscopic levels of the isolated Pt atom and singly ionized ions. The latter is achieved by the modification of the onsite energy function. The scalar-relativistic version, SR-SCTB, is very successful in describing properties of platinum surfaces (we considered ⟨001⟩, ⟨011⟩, ⟨111⟩, ⟨310⟩, ⟨210⟩ surfaces and reconstructions of ⟨001⟩ and ⟨011⟩ faces). Energetics, atomic displacements and reconstructions are good agreement with available first principles calculations and experiments. New results on the $5\times$ 29 reconstruction of the ⟨001⟩ Pt surface, which is too large for DFT calculations, are consistent with experimental suggestions that the reconstruction is more stable than the 5×1 reconstruction[42]. The full relativistic model SO-SCTB gave a much larger surface energy for the missing row reconstruction of the ⟨011⟩ surface than that obtained from the SR-SCTB model, consistent with earlier claims[39] that relativistic effects are required to stabilize this structure. The full SO-SCTB model is about an order of magnitude faster than first principles DFT calculations which use a less complete description of the relativistic effects and it requires roughly ten times less memory.

In future work, we will use parametrizations characterizing oxygen and hydrogen entities in these SCTB models, so that oxygen dissociation and reduction and successive protonation of bound oxygen in the presence of water can be studied using these methods.

VI. ACKNOWLEDGEMENTS

This work was supported by a subcontract to the University of Minnesota from Argonne National Laboratory, prime Department of Energy contract W-31-109-ENG38.

Appendix: Detailed description of the fitting procedure for the fully relativistic model

To parametrize the SO-SCTB model we only need to change the parametrization of the onsite function because the SR-SCTB model described in section II implicitly contains scalar-relativistic effects in the SR-VASP database and in the ionization potentials. As described above, we fit the onsite energy function $E_{I,\infty}(\{Q\},\{n\},J_I)$ to the lowest lying many body energy eigenstates of the isolated Pt ions, taking the set $\{n\}$ to be the occupation numbers of the $5d_{5/2}$ and $5d_{3/2}$ orbitals. In the Hartree Fock approximation including the spin orbit interaction, the many body states of the neutral Pt atom can be described in jj-coupling by configurations $5d_{3/2}^{n_{3/2}}5d_{5/2}^{n_{5/2}}6s^{n_s}$ and states

involving p orbitals which we ignore. Here $n_{3/2}+n_{5/2}+n_s=10$ and $0\le n_{3/2}\le 4, 0\le n_{5/2}\le 6$ and $0\le n_s\le 2$, corresponding to 2 holes in the s and d valence shells. There are 6 configurations consistent with these constraints. In jj-coupling, each of these configurations will lead to states corresponding to several values of total J and there will be states corresponding to the same J arising from different configurations. However the low lying states can be distinguished by specifying $n_{3/2}, n_{5/2}$ and J as shown in the first three columns of Table VI. (n_s is fixed if $n_{3/2}, n_{5/2}$ are, within this set of configurations.) Unfortunately, though jj-coupling is the appropriate approximation scheme for platinum, experimental energy levels are reported in some cases using term notation appropriate to LS-coupling[53]. In those cases, some ambiguity can arise concerning which state associated with a combination $n_{3/2}, n_{5/2}, J$ should be associated with a state labeled with an LS term derived from a configuration described by a configuration $5d^{n_d}6s^{n_s}$. We dealt with these ambiguities by expanding the two hole states derived from the jj basis in terms of two hole states in the LS basis and then identified states in the jj basis with those LS terms which had the largest coefficients in the expansion.

General states of n electrons are formed in the following manner in LS-coupling. ($|LSJM\rangle$ is the state with total angular momentum J and $J_z=M$ formed from the states with total angular momentum L and total spin S in LS coupling)

$$|LSJM\rangle = (((((l_1;l_2)L_2;l_3)L_3;...;l_n)L_n)((((s_1;s_2)S_2;s_3)S_3;...;s_n)S_n))JM \tag{21}$$

Here l_i, s_i are the orbital momentum and spin of the individual Hartree-Fock orbitals. The notation means that the orbital states with l_1, l_2 are first combined to form states of orbital L_2. Then the two electron states with orbital L_2 are combined with one electron states with orbital l_3 to form three electron states with orbital angular momentum L_3 and so forth to form a purely orbital wave function with total orbital angular momentum L_n. A similar process produces spinor states with total spin angular momentum S_n and the states with total L_n, S_n are combined to form states of J, M. By contrast in $jj-$coupling the basis states of J, M formed as indicated by

$$|jjJM\rangle = ((((l_1,s_1)j_1;(l_2,s_2)j_2)J_2;(l_3,s_3)j_3)J_3;...;(l_n,s_n)j_n)JM \tag{22}$$

in a similar notation. Here j_i is the total angular momentum of an individual electron orbital and J_k is the intermediate total momentum of orbitals with $i\le k$. States in both of these schemes span the same vector space using different basis sets. Therefore one can express states in one scheme in terms of states in the other.

$$|jjJM\rangle = \sum_{\{L,S\}} T_{jjJM,LS}|LSJM\rangle \tag{23}$$

where the summation goes over all combinations of l_i,s_i,L_i and S_i, that produce the same final J value. The procedure to compute the coefficients $T_{jjJM,LS}$ is given, for example, in[24], but references[54,55] provide a closed form formula for the coefficients $T_{jjJM,LS}$ for n electrons which we reproduce here

$$T_{jjJM,LS} = \prod_{i=2}^{n}(2L_i+1)^{\frac{1}{2}}(2S_i+1)^{\frac{1}{2}}(2J_{i-1}+1)^{\frac{1}{2}}(2j_i+1)^{\frac{1}{2}}\begin{Bmatrix} L_{i-1} & l_i & L_i \\ S_{i-1} & s_i & S_i \\ J_{i-1} & j_i & J_i \end{Bmatrix} \tag{24}$$

where the expression in {} is a $9j$ symbol[54].

We will illustrate the use of this formula for the case of two electrons (equivalent to two holes: the neutral Pt case). The ground state of neutral Pt is characterized by J=3 and hole occupation of $5d^16s^1$. Therefore these holes have the following quantum numbers: $l_1=2, s_1=1/2$ and $l_2=0, s_2=1/2$. Therefore for LS-coupling $L_2=2,\ S_2=0,1$ and $J=3$ can be obtained only by taking $L_2=2, S_2=1$. Similarly, in jj-coupling $j_1=3/2,5/2,\ j_2=1/2$ and making a $J=3$ state is possible only by using $j_1=5/2,\ j_2=1/2$. Hence for $J=3$, no calculation is necessary and the ground state is identified as $J=3$, $n_{5/2}=5$(one $j=5/2$ hole) and $n_{3/2}=4$ (no $j=3/2$ holes).

On the other hand, with two holes, total angular momentum of $J=2$ can be obtained in two different ways in both schemes:. In LS-coupling both $L_2=2,\ S_2=0$ and $L_2=2,\ S_2=1$ can give a $J=2$ state , while in jj-coupling: $j_1=3/2,\ j_2=1/2$ and $j_1=5/2,\ j_2=1/2$ can both form a $J=2$ state. For this case of 2 holes and $J=2$ the product in Eq. [24] consists of only one factor, and we have for the transformation coefficients

$$T_{\frac{5}{2}\frac{1}{2}2M,20} = (2\cdot 2+1)^{\frac{1}{2}}(2\cdot 0+1)^{\frac{1}{2}}(2\cdot\frac{5}{2}+1)^{\frac{1}{2}}(2\cdot\frac{1}{2}+1)^{\frac{1}{2}}\begin{Bmatrix} 2 & 0 & 2 \\ \frac{1}{2} & \frac{1}{2} & 0 \\ \frac{5}{2} & \frac{1}{2} & 2 \end{Bmatrix} = \sqrt{60\cdot\frac{1}{100}} = \sqrt{\frac{3}{5}}$$

$$T_{\frac{3}{2}\frac{1}{2}2M,20} = (2\cdot 2+1)^{\frac{1}{2}}(2\cdot 0+1)^{\frac{1}{2}}(2\cdot\frac{3}{2}+1)^{\frac{1}{2}}(2\cdot\frac{1}{2}+1)^{\frac{1}{2}}\left\{\begin{array}{ccc} 2 & 0 & 2 \\ \frac{1}{2} & \frac{1}{2} & 0 \\ \frac{3}{2} & \frac{1}{2} & 2 \end{array}\right\} = -\sqrt{40\cdot\frac{1}{100}} = -\sqrt{\frac{2}{5}}$$

$$T_{\frac{5}{2}\frac{1}{2}2M,21} = (2\cdot 2+1)^{\frac{1}{2}}(2\cdot 1+1)^{\frac{1}{2}}(2\cdot\frac{5}{2}+1)^{\frac{1}{2}}(2\cdot\frac{1}{2}+1)^{\frac{1}{2}}\left\{\begin{array}{ccc} 2 & 0 & 2 \\ \frac{1}{2} & \frac{1}{2} & 0 \\ \frac{5}{2} & \frac{1}{2} & 2 \end{array}\right\} = \sqrt{180\cdot\frac{1}{450}} = \sqrt{\frac{2}{5}}$$

$$T_{\frac{3}{2}\frac{1}{2}2M,21} = (2\cdot 2+1)^{\frac{1}{2}}(2\cdot 1+1)^{\frac{1}{2}}(2\cdot\frac{3}{2}+1)^{\frac{1}{2}}(2\cdot\frac{1}{2}+1)^{\frac{1}{2}}\left\{\begin{array}{ccc} 2 & 0 & 2 \\ \frac{1}{2} & \frac{1}{2} & 0 \\ \frac{3}{2} & \frac{1}{2} & 2 \end{array}\right\} = \sqrt{120\cdot\frac{1}{200}} = \sqrt{\frac{3}{5}}$$

Thus from equation [24],

$$|5/2\ 1/2\ 2M>= \sqrt{\frac{3}{5}}|D_2^1 M> + \sqrt{\frac{2}{5}}|D_2^3 M>$$

$$|3/2\ 1/2\ 2M>= -\sqrt{\frac{2}{5}}|D_2^1 M> + \sqrt{\frac{3}{5}}|D_2^3 M>$$

So for $J=2$ and two holes, choosing the largest coefficient in each case, we identify the spectroscopic experimental state labelled $L=2,\ S=0$ (LS term $^1\mathrm{D}_2$) with electron occupation numbers associated with one $5/2$ hole and no $3/2$ holes corresponding to $n_{5/2}=5,\ n_{3/2}=4$, while the spectroscopic state labelled $L=2,\ S=1$ (LS term $^3\mathrm{D}_2$) is identified with one $3/2$ hole and no $5/2$ holes corresponding to $n_{5/2}=6,\ n_{3/2}=3$.

Application to systems with three electrons or more is straightforward. We used[56] for the $9j$ symbol computations.

The resulting correspondences of the various values of $n_{3/2}, n_{5/2}, J$ with the experimental levels labeled with LS configurations and terms is shown in columns 4 and 5 of Table VI and the corresponding energies used in the database for fitting the SCTB model are shown in the last column.

For singly ionized platinum Pt+ there are three holes in the $5d6s$ shell and fixing $n_{3/2}, n_{5/2}$ and J does not uniquely identify the states. However because the states of Pt^+ all lie substantially higher than the neutral Pt states, we chose, in cases of ambiguity, to associate the state with lowest energy with the set $n_{3/2}, n_{5/2}, J$.

TABLE VI: Low energy spectrum of neutral platinum atom.

$n_{3/2}$	$n_{5/2}$	J	LS hole conf.	LS term	Energy(eV)
4	5	3	$5d^1 6s^1$	$^3D_3$	0.0000
3	6	2	$5d^1 6s^1$	$^3D_2$	0.0962
4	4	4	$5d^2 6s^0$	$^3F_4$	0.1032
4	6	0	$5d^0 6s^2$	$^1S_0$	0.7612
3	5	2	$5d^2 6s^0$	$^3P_2$	0.8143
3	5	3	$5d^2 6s^0$	$^3F_3$	1.2543
3	6	1	$5d^1 6s^1$	$^3D_1$	1.2562
4	5	2	$5d^1 6s^1$	$^1D_2$	1.6733
3	6	2	$5d^1 6s^1$	$^3F_2$	1.9221
3	6	0	$5d^2 6s^0$	$^3P_0$	2.1058
3	5	1	$5d^2 6s^0$	$^3P_1$	2.3020
3	5	4	$5d^2 6s^0$	$^3G_4$	2.7237
4	4	2	$5d^2 6s^0$	$^1D_2$	3.3029

TABLE VII: Low energy spectrum of singly positively ionized platinum atom.

$n_{3/2}$	$n_{5/2}$	J	LS hole conf.	LS term	Energy(eV)
4	5	5/2	$5d^1 6s^0$	$^2D_{5/2}$	0.000
3	6	3/2	$5d^1 6s^0$	$^2D_{3/2}$	1.044
4	4	9/2	$5d^2 6s^1$	$^4F_{9/2}$	0.593
3	5	7/2	$5d^2 6s^1$	$^4F_{7/2}$	1.160
3	5	5/2	$5d^2 6s^1$	$^4F_{5/2}$	1.653
2	6	3/2	$5d^2 6s^1$	$^4F_{3/2}$	1.958
3	5	5/2	$5d^2 6s^1$	$^4P_{5/2}$	2.086
3	5	3/2	$5d^2 6s^1$	$^4P_{3/2}$	2.625
3	5	1/2	$5d^2 6s^1$	$^4P_{1/2}$	2.693
4	4	7/2	$5d^2 6s^1$	$^2F_{7/2}$	2.244
2	6	5/2	$5d^2 6s^1$	$^2F_{5/2}$	2.909
4	4	3/2	$5d^2 6s^1$	$^2D_{3/2}$	2.960
4	4	5/2	$5d^2 6s^1$	$^2D_{5/2}$	4.085
2	6	1/2	$5d^2 6s^1$	$^2P_{1/2}$	3.379
3	5	3/2	$5d^2 6s^1$	$^2P_{3/2}$	3.997
3	5	7/2	$5d^2 6s^1$	$^2G_{7/2}$	3.599
3	5	9/2	$5d^2 6s^1$	$^2G_{9/2}$	3.628

TABLE VIII: Low energy spectrum of singly negatively ionized platinum atom.

$n_{3/2}$	$n_{5/2}$	J	LS hole conf.	LS term	Energy(eV)
4	5	5/2	$5d^1 6s^0$	$^2D_{5/2}$	0.000
3	6	3/2	$5d^1 6s^0$	$^2D_{3/2}$	1.244

Energies of the ionization states +2, +3 and +4 of platinum were assigned their ionization potential values, independent of the values of $n_{3/2}, n_{5/2}, J$.

After experimenting with various ways to parametrize this data base of the energies $E_\infty(Q, n_{3/2}, n_{5/2}, J)$ of states of the isolated Pt atom, we found that a representation of the dependence on $n_{3/2}, n_{5/2}, J$ by a set of gaussian functions

and of the dependence on charge by a polynomial in Q was satisfactory. The parametrization of $E_\infty(Q, n_{3/2}, n_{5/2}, J)$ at discrete values $m|e|$ of the charge Q was written in the form

$$E_\infty(Q = m|e|, n_{3/2}, n_{5/2}, J) = C_m - \sum_{terms\ i} B_i e^{(w_m((n_{3/2}-n_{i,3/2})^2+(n_{5/2}-n_{i,5/2})^2+(J-J_i)^2))} \tag{25}$$

containing parameters C_m, B_i and w_m. Note that, in this form, the parameters C_m and B_i are completely fixed by the charge on the Pt and by the spectroscopic values of the term energies, since for the isolated ions, $n_{i,3/2} = n_{3/2}$ $n_{5/2} - n_{i,5/2}$,$J = J_i$. However, this fit to the spectroscopic terms does not determine the values of the parameters w_m which parametrize the changes in onsite energies which occur when these variables are not at their 'stoichiometric' values in the solid. To determine the w_m we were forced to utilize results from the first principles SO-VASP calculations on bulk Pt as described in section II, resulting a procedure which is not completely consistent. During the fit to the SO-VASP determined cohesive energies and bands we used parameters determining the $t_{I\mu,K\nu}$ (Eq. [2]) and E_{env} (coefficients A_n) from the SR- SCTB model, and parameters C_m and and B_i $E_{I,\infty}(\{Q\}, \{n\}, J_I)$ from the fit to spectroscopic levels so that only the w_m were varied in the fit.

This fitting step required values of E_∞ at values of Q other than $Q = m|e|$ with $-1 \leq m \leq 4$ and these were obtained by fitting the values at the discrete values of Q to a polynomial. At the next step in the fit, with the values of all the parameters except the B_i fixed, we adjusted the B_i so that the energies E_∞ given by the above expression matched the values for isolated Pt ions given in Tables II-IV and for the higher cationic states as described above. (This determination of B_i's simply required a matrix inversion.) Then the w_m were varied to optimize the fit to the SO-VASP results. The last step is the only one in which the SO-VASP data base is used. Because the manner in which the SO coupling is treated in the SO-VASP calculation[31] is different than in our SO-SCTB parametrization, the procedure is not fully consistent and the fact that the SO-SCTB and SO-VASP cohesive energies and bands do not match extremely well is unsurprising.

The energy surface for the neutral platinum atom which results from these assumptions is shown in Fig. 11 for $J = 0, 1, 2, 3, 4$ and for the singly ionized atom in Fig. 12 for $J = 1/2, 3/2, 5/2, 7/2$ and $9/2$.

[1] F. Zaerai, Surf. Sci. 500, 947 (2002)
[2] T. Li and P. B. Balbuena, Chem. Phys. Lett. 367,439 (2003)
[3] J. K. Norskov, J. Rossmeisi, A. Logadottir L. Linqvist, J. R. Kitchin, T. Bligaard and H. Jonsson, J. Phys. Chem. 108, 17886 (2004)
[4] J. Greeley and M. Mavrikakis, J. Am. Chem. Soc.124, 7193 (2002)
[5] S. K. Desai, M. Neurock, K. Kourtakis, J. Phys. Chem. B 106, 2559 (2002)
[6] S. K. Desai and M. Neurock, Phys. Rev, B68, 075420 (2003)
[7] G. Seifert, H.-G. Fritsche, P. Ziesche and V. Heera, Phys. Stat. Sol. B **121** 705 (1984).
[8] G. Pacchioni, S.-C. Chung, S. Kruger, N. Rausch, Surf. Sci. **392** 173 (1997).
[9] R. G. Boyd, A. C. Larson and J. T. Waber, Phys. Rev. **12 9**, 1629 (1962).
[10] N. Yu and J. W. Halley, Materials Science Forum 185-188, 389 (1995)
[11] P. Schelling, N.Yu and J.W.Halley, Phys. Rev. B. **58**, 1279 (1998).
[12] P. Schelling and J. W. Halley, Phys. Rev. B62, 3241 (2000)
[13] J. W. Halley, P. K. Schelling and M. Zhuang, in "Proceedings of the Third Recontres du Vietnam: Superconductivity, Magneto-Resistive Materials and Strongly Correlated Systems", Nguyen Van Hieu, Tran Thanh Van and Gang Xiao, eds. Vietnam National University Press (2000) p. 137
[14] Min Zhuang and J. W. Halley, Physical Review B 64, 024413 (2001)
[15] P. Schelling and J. W. Halley J. W. Halley, ed. ACS publications (2001) p.142
[16] J. W. Halley, Y. Lin and M. Zhuang , Farad. Discuss 212, 85-95 (2002)
[17] J. W. Halley, S. Erdin, Y.Lin and Peter Zapol, in Proceedings of CMT27 , Nova 27th International Workshop on Condensed Matter Theories (CMT-27), SEP 15-20, 2004, Condensed Matter Theories 19 , 61-68 (2005)
[18] A. S. Barnard, S. Erdin, Y. Lin, P. Zapol and J. W. Halley, Phys. Rev. B 73, 205405 (2006)
[19] Serkan Erdin, Y. Lin and J. Woods Halley, Phys. Rev. B72, 035405 (2005)
[20] J. Woods Halley, Serkan Erdin, You Lin, Peter Zapol, , Journal of Electroanalytical Chemistry 607, 147 (2007)
[21] V. Theileis and H. Bross, Phys. Rev. B62, 13338 (2000)
[22] C. Leahy, M. Yu, C.S. Jayanthi and S.Y. Wu, Phys. Rev. B, **74**, 155408 (2006).
[23] P. Pyykko, Chem. Rev. **88**, 563 (1988).
[24] E. U. Condon,G. H. Shortley, "The Theory of Atomic Spectra" Cambridge University Press, (1935).
[25] G. Kresse and J. Hafner, Phys. Rev. B, **47**, 558 (1993).
[26] G. Kresse and J. Furthmuller, Comput. Mat. Sci, **6**, 15 (199 6).
[27] G. Kresse and J. Furthmuller, Phys. Rev. B, **54**, 11169 (199 4).
[28] Gaussian 03, Revision C.02, M. J. Frisch, G. W. Trucks, H. B. Schlegel, G. E. Scuseria, M. A. Robb, J. R. Cheeseman, J. A. Montgomery, Jr., T. Vreven, K. N. Kudin, J. C. Burant, J. M. Millam, S. S. Iyengar, J. Tomasi, V. Barone, B. Mennucci, M. Cossi, G. Scalmani, N. Rega, G. A. Petersson, H. Nakatsuji, M. Hada, M. Ehara, K. Toyota, R. Fukuda, J. Hasegawa, M. Ishida, T. Nakajima, Y. Honda, O. Kitao, H. Nakai, M. Klene, X. Li, J. E. Knox, H. P. Hratchian, J. B. Cross, V. Bakken, C. Adamo, J. Jaramillo, R. Gomperts, R. E. Stratmann, O. Yazyev, A. J. Austin, R. Cammi, C. Pomelli, J. W. Ochterski, P. Y. Ayala, K. Morokuma, G. A. Voth, P. Salvador, J. J. Dannenberg, V. G. Zakrzewski, S. Dapprich, A. D. Daniels, M. C. Strain, O. Farkas, D. K. Malick, A. D. Rabuck, K. Raghavachari, J. B. Foresman, J. V. Ortiz, Q. Cui, A. G. Baboul, S. Clifford, J. Cioslowski, B. B. Stefanov, G. Liu, A. Liashenko, P. Piskorz, I. Komaromi, R. L. Martin, D. J. Fox, T. Keith, M. A. Al-Laham, C. Y. Peng, A. Nanayakkara, M. Challacombe, P. M. W. Gill, B. Johnson, W. Chen, M. W. Wong, C. Gonzalez, and J. A. Pople, Gaussian, Inc., Wallingford CT, 2004.
[29] J.A. Pople, M. Head-Gordon, and K. Raghavachari, J. Chem. Phys. **87**, 5968 (1987).
[30] J. Thogersen, L.D. Steele, M. Scheer, C.A. Brodie and H. K. Haugen, J.Phys. B. **29**, 1323 (1996).
[31] Yoon-Suk Kim, Kerstin Hummer, and Georg Kresse Physical Review B 80, 035203 (2009).
[32] J.P.Perdew and A.Zunger, Phys. Rev. B. **23**, 5048 (1981).
[33] M. C. Payne, M. P. Teter, D. C. Allan, T. A. Arias, and J. D. Joannopoulus, Rev. Mod. Phys. **64**, 1045 (1992).
[34] S. Baud and C. Ramseyer and G. Bihlmayer and S. Blugel and C . Barreteau and M. C. Desjonqueres and D. Spanjaard and N. Bernstein, Phys. Rev. B **70**, 235423 (2004).
[35] P. Feibelman, Physical Review B 52, 16845 (1995).
[36] V. Zolyomi and L. Vitos and S. K. Kwon and J. Kollar,J. Phys: Condens. Matter **21**, 095007 (2009).
[37] J. C. Boettger, Phys. Rev. B **49** 16798 (1994)
[38] J. Wiebe, F. Meier, K. Hashimoto, G. Bihlmayer, S. Blugel, P.Ferriani, S. Heinze, R. Weisenberger, Physical Review B 72, 193406 (2005)
[39] S. Olivier, G. Treglia, A. Saul and F. Willaime, Surf. Sci. **600** 5131 (2006).
[40] M. A. Van Hove, R. J. Koestner, P. C. Stair, J. P. Biberi an, L. L. Kesmodel, I. Bartos and G. A. Somorjai, Surf. Sci. **103** 189 (1981).
[41] Y. Y. Yeo, C. E. Wartnaby and D. A. King, Science **268** 1731 (1995).
[42] K. Heinz, E. Lang, K. Strauss and K. Mller, Appl. Surf. Sci., **11-12** 611 (1982).
[43] P. Heilmann, K. Heinz and K. Mller, Surf. Sci., **83** 487 (1979).
[44] J. J. Mortensen, T. R. Linderoth, K. ,W. Jacobsen, E. Lagsgaard, I. Stensgaard, and F. Besenbacher, Surf. Sci., **400** 290 (1998).

[45] G. Ritz, M. Schimd, P. Varga, A. Borg and M. Ronning, Phys. Rev. B., **56** 10518 (1997).
[46] V. Fiorentini, M. Methfessel and M. Scheffler, Phys. Rev. Lett. **71** 1051 (1993).
[47] N. A. Deskins, J. Lauterbach and K. T. Thomson, J. of Chem. Phys. **122** 184709 (2005).
[48] P. van Beurden and G. J. Kramer, J. of Chem. Phys. **121** 2317 (2004).
[49] C. S. Chang, W. B. Su, C. M. Wei and T. T. Tsong, Phys. Rev. Lett. **83** 2604 (1999).
[50] K. Wandelt, Surf. Sci. **251/252**, 387 (1991).
[51] Y. Y. Sun, H. Xu, Y. P. Feng, A. C. H. Huan and A. T. S. Wee, Surf. Sci. **548**, 309 (2004).
[52] A. Kokalj and M. Caus, J. Phys. Condens. Matter **11**, 7463 (1999).
[53] C.E. Moore, *Atomic Energy Levels*, Natl. Bur. Stand. (U.S.)Circ. 467, (1959).
[54] R. D. Cowan, "The Theory of Atomic Structure and spectra", p. 2 49.
[55] R. D. Cowan, J. Opt. Soc. Am. **58**, 808 (1968).
[56] http://plasma-gate.weizmann.ac.il/369j.html.

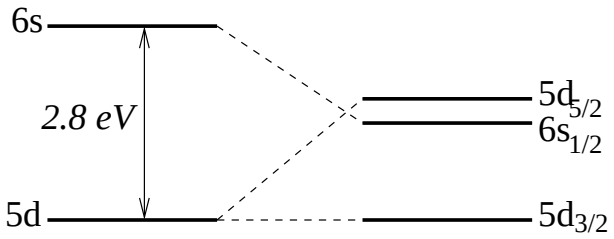

FIG. 1: Schematic representation of the valence shell of Pt atom with (right panel) and without (left panel) relativistic effects: there is a qualitative change in the electronic structure.

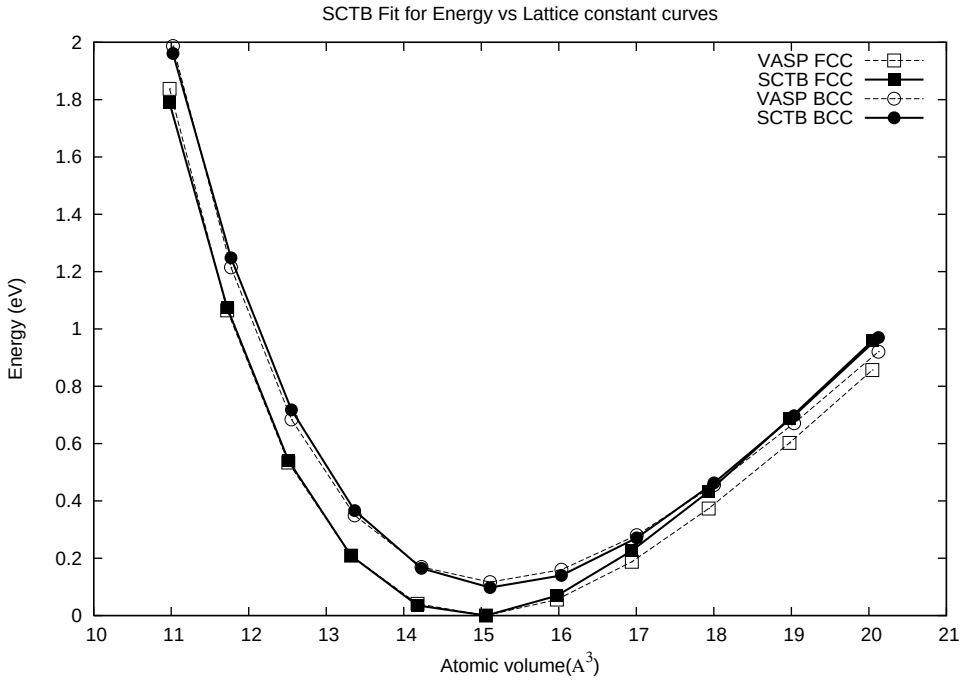

FIG. 2: Cohesive energy (relative to the ground state) of the FCC and BCC Pt as calculated by SR-VASP and SR-SCTB as a function of atomic volume.

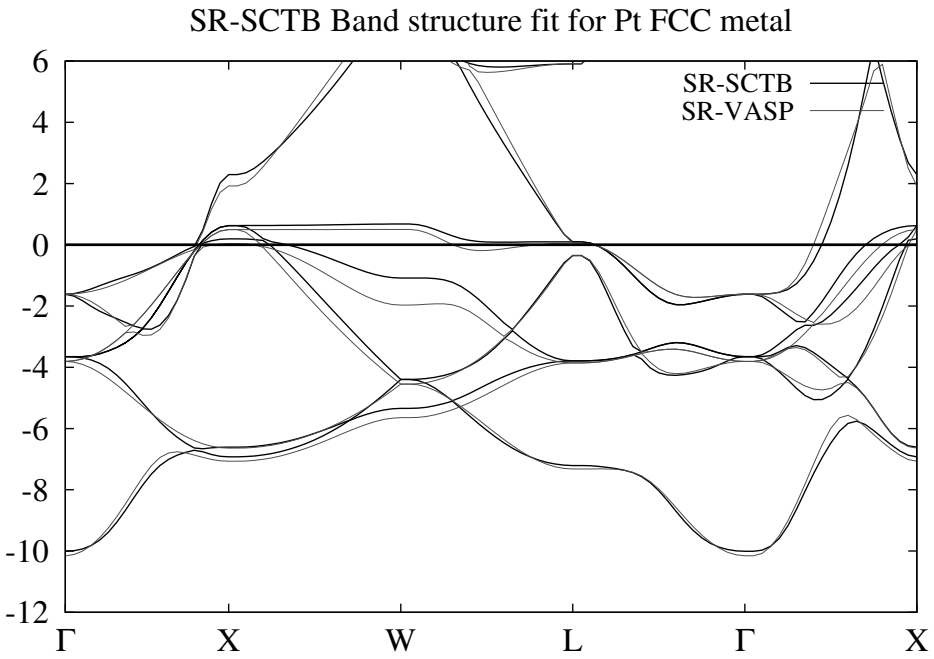

FIG. 3: Comparison of the electronic band structures between SR-VASP calculations and the SR-SCTB model for FCC Pt

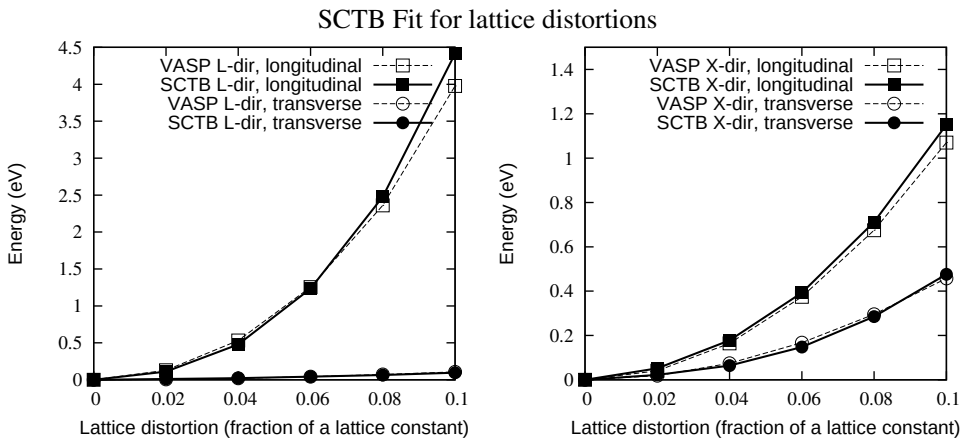

FIG. 4: Cohesive energy as a function of lattice distortions: comparison between SR-VASP and SR-SCTB. Panel A: distortion along L-direction, Panel B: Distortion along X-direction

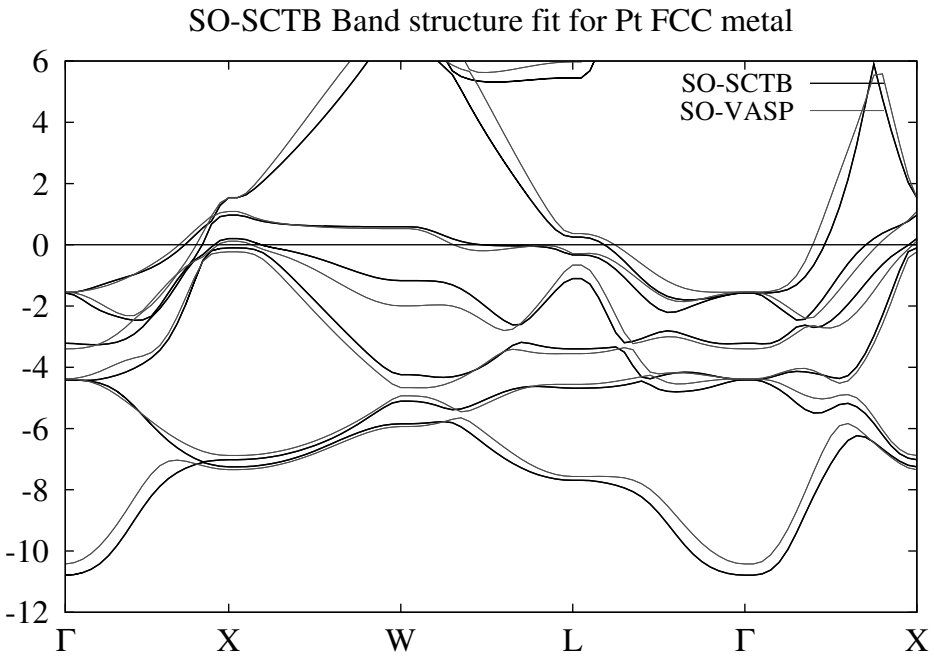

FIG. 5: Comparison of the electronic band structures between SO-VASP calculations and SO-SCTB model for FCC Pt. Note the characteristic splitting of the d-band at the gamma point of $\sim 1\ eV$

.

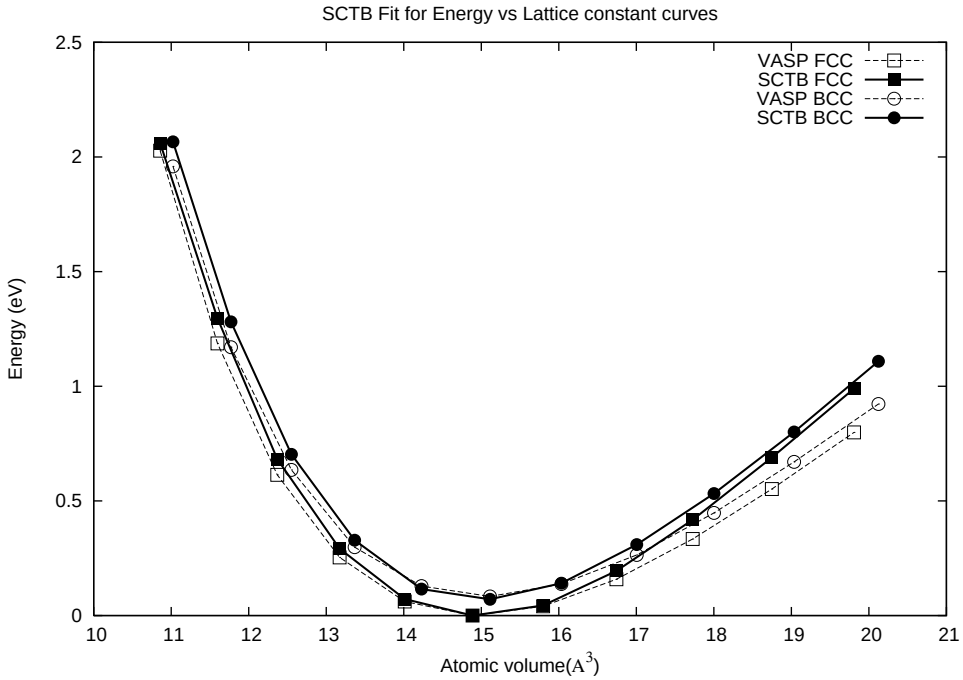

FIG. 6: Cohesive energy (relative to the ground state) of the FCC and BCC Pt as calculated by SO-VASP and relativistic SO-SCTB as a function of atomic volume.

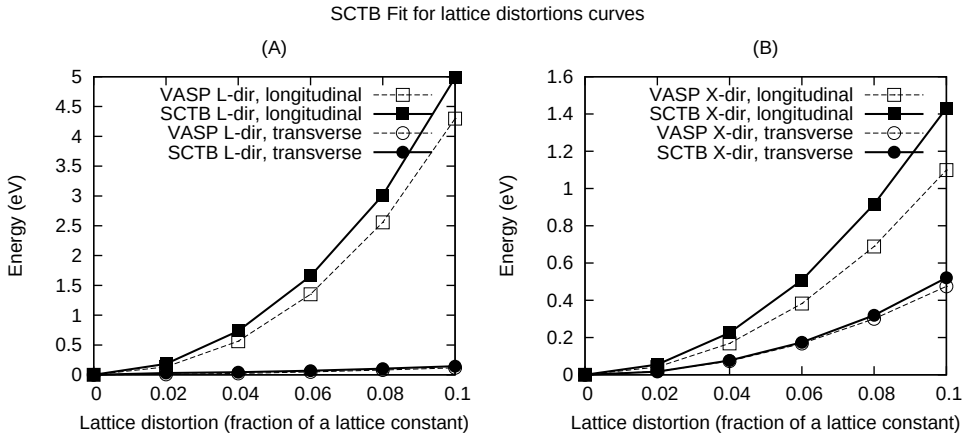

FIG. 7: Cohesive energy as a function of lattice distortions: comparison between SO-VASP and SO-SCTB. Panel A: distortion along L-direction, Panel B: Distortion along X-direction

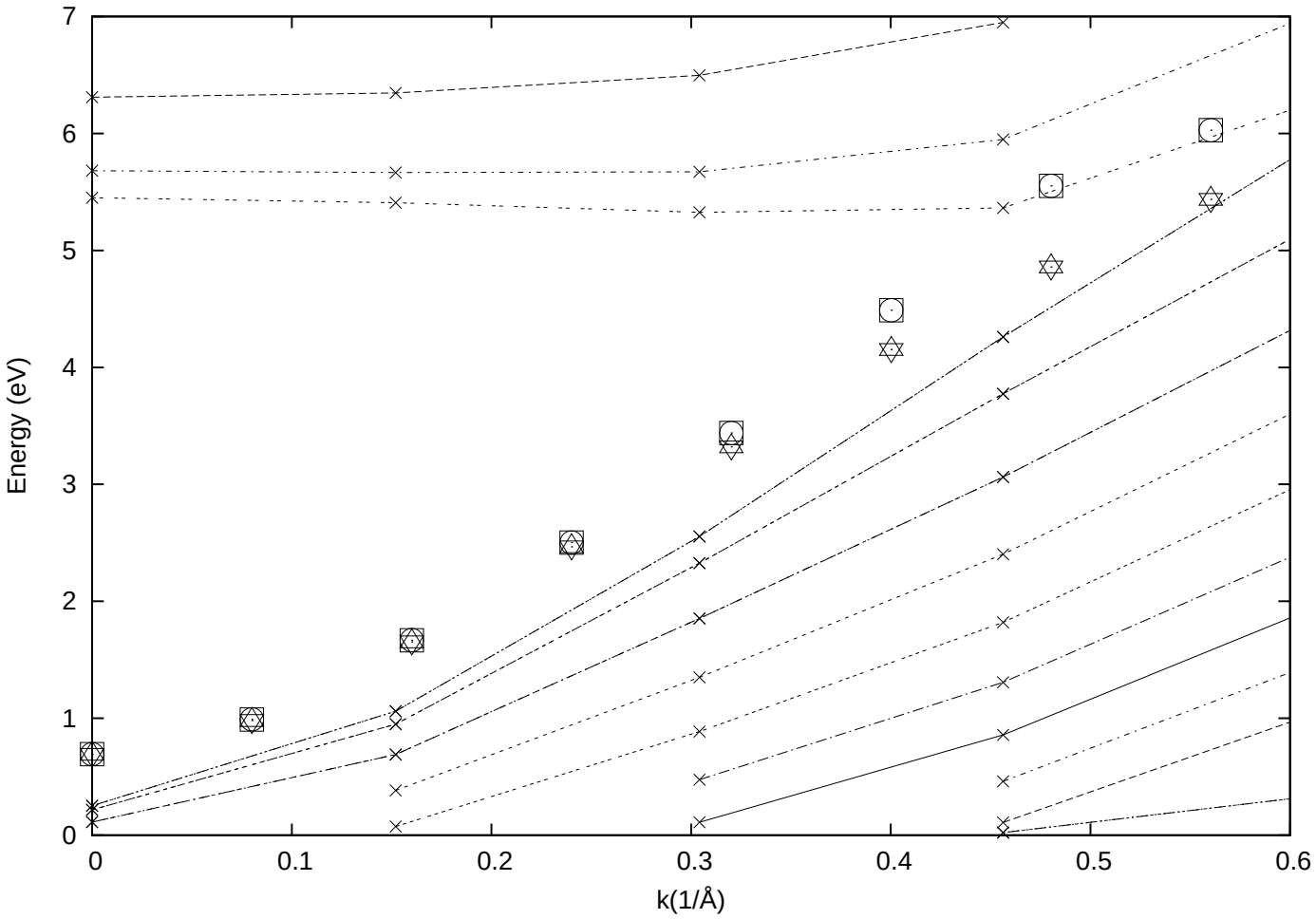

FIG. 8: Energy of surface states (points) from eigenvectors of the effective one electron Hamilton for SO-SCTB for a 24 layer slab terminated in the 111 direction. The k-vectors are along the $\bar{\Gamma}$-$\bar{K}$ direction in the 111 surface Brillouin zone as defined in reference[38]. The points connected by lines show the energies of Pt bulk band states projected onto the 111 surface zone as calculated in the SO-SCTB model. Compare Figure 4a of reference[38].

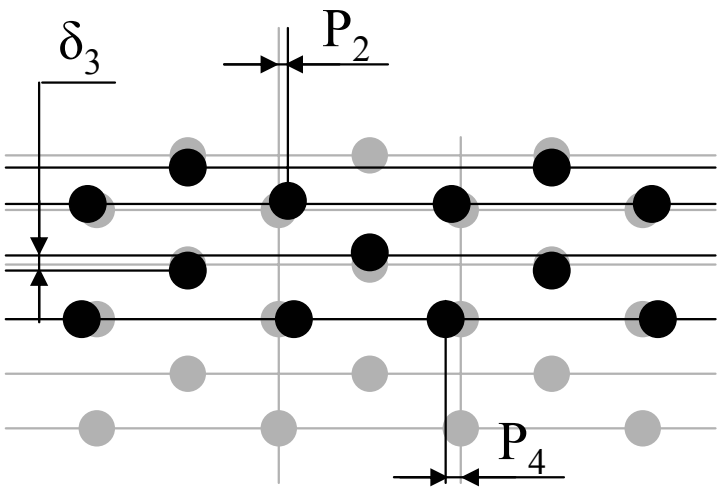

FIG. 9: Positions of the atoms for the ⟨011⟩ missed row reconstruction. Grey atoms show ideal positions, while black are the actual positions. For the value of the structural parameters see Table III.

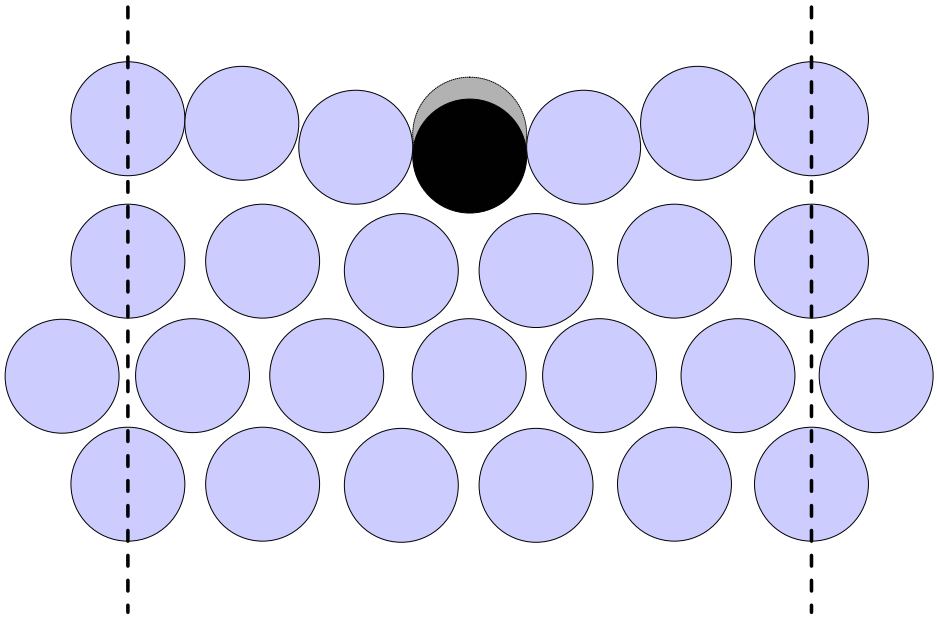

FIG. 10: Unit cell for the 5×1 model of hexagonal reconstruction. Atom in the center of symmetry has different equilibrium position in calculations with SR-SCTB (black) and DFT simulations (references 44,45, grey).

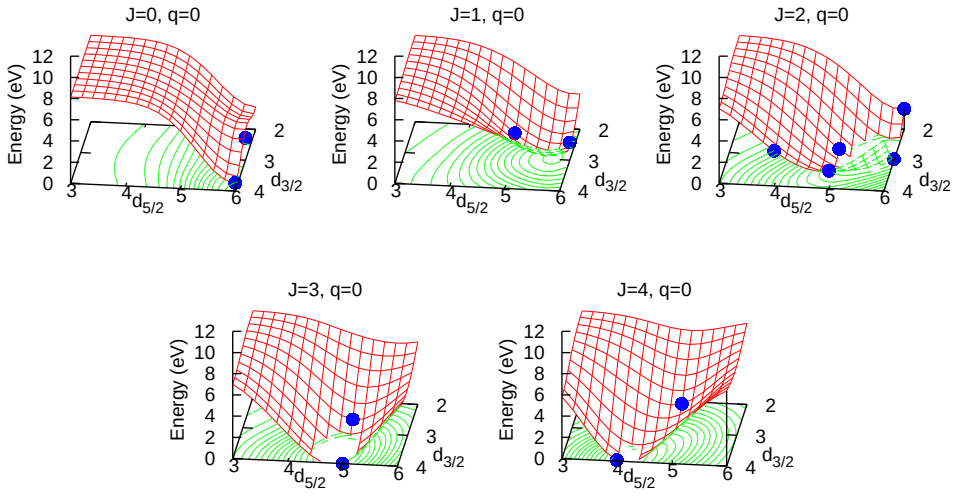

FIG. 11: Example of the fit of the onsite energy function for the SO-SCTB Pt model. Energy surface in $5d_{3/2}$,$5d_{5/2}$ coordinates is shown with q=0 and J=0,1,2,3,4.

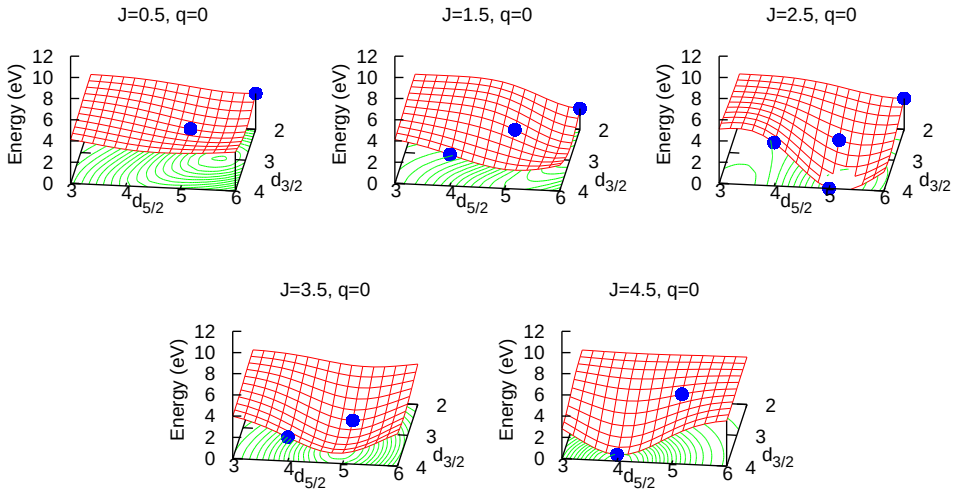

FIG. 12: Example of the fit of the onsite energy function for the SO-SCTB Pt model. Energy surface in $5d_{3/2}$,$5d_{5/2}$ coordinates is shown with q=0 and J=1/2,3/2,5/2,7/2,9/2.